Cao *et al. Soft Sci* 2023;3:32
DOI: 10.20517/ss.2023.22

Soft Science

Research Article

Open Access

Flexible tactile sensor with an embedded-hair-in-elastomer structure for normal and shear stress sensing

Yudong Cao, Jiacheng Li, Zihao Dong, Tianyu Sheng, Deyuan Zhang, Jun Cai, Yonggang Jiang*

Insitute of Bionic and Micro-nano Systems, School of Mechanical Engineering and Automation, Beihang University, Beijing 100191, China.

***Correspondence to:** Prof. Yonggang Jiang, Insitute of Bionic and Micro-nano Systems, School of Mechanical Engineering and Automation, Beihang University, Beijing 100191, China. E-mail: jiangyg@buaa.edu.cn

How to cite this article: Cao Y, Li J, Dong Z, Sheng T, Zhang D, Cai J, Jiang Y. Flexible tactile sensor with an embedded-hair-in-elastomer structure for normal and shear stress sensing. *Soft Sci* 2023;3:32. https://dx.doi.org/10.20517/ss.2023.22

Received: 10 May 2023 **First Decision:** 21 Jun 2023 **Revised:** 11 Jul 2023 **Accepted:** 21 Jul 2023 **Published:** 7 Oct 2023

Academic Editor: Zhifeng Ren **Copy Editor:** Pei-Yun Wang **Production Editor:** Pei-Yun Wang

Abstract
Endowing robots with multi-directional tactile sensing capabilities has long been a challenging task in the field of flexible electronics and intelligent robots. This paper reports a highly sensitive, flexible tactile sensor with an embedded-hair-in-elastomer structure, which is capable of decoupling normal stress and shear stress. The flexible tactile sensor is fabricated on a thin polyimide substrate and consists of four self-bending piezoresistive cantilevers in a cross-shaped configuration, which are embedded in an elastomer. The sensor can decouple the tactile information into a normal stress and a shear stress with simple summation and differencing algorithms, and the measurement error is kept within 3%. Moreover, the sensitivity and detection threshold of the sensor can be adjusted by simply changing the elastic material. As a demonstration, the flexible tactile sensor is integrated into a robotic manipulator to precisely estimate the weight of the grasped objects, which shows great potential for application in robotic systems.

Keywords: Tactile sensor, piezoresistive cantilever, flexible sensor, intelligent robot

INTRODUCTION

Over the past decades, the application of robots has expanded from industrial robots that perform repetitive and limited tasks to Tri-Co Robots that can learn autonomously and interact with humans and

© The Author(s) 2023. **Open Access** This article is licensed under a Creative Commons Attribution 4.0 International License (https://creativecommons.org/licenses/by/4.0/), which permits unrestricted use, sharing, adaptation, distribution and reproduction in any medium or format, for any purpose, even commercially, as long as you give appropriate credit to the original author(s) and the source, provide a link to the Creative Commons license, and indicate if changes were made.

Cao *et al. Soft Sci* 2023;3:32 | https://dx.doi.org/10.20517/ss.2023.22

environments[1,2]. The robotic system interacts with the environment mainly based on visual and haptic information[3]. For haptic feedback and dexterous manipulation, various tactile sensors have been developed. However, the development of flexible tactile sensors with tri-axial sensing capabilities remains a great challenge.

Significant efforts have been made in the development of tactile sensors based on a variety of sensing mechanisms[4], including piezoresistive[5-9], piezoelectric[10-13], capacitive[14-17], magnetic[18-22], and optical[23] sensors. In particular, the piezoresistive mechanism is widely used because of its simple device structure, well-established read-out mechanism, and convenient signal acquisition. To endow robots with haptic feedback, tri-axial piezoresistive tactile sensors have been one of the focuses in the field of Tri-Co Robots. Takahashi *et al.* proposed a tri-axial tactile sensor consisting of three pairs of silicon (Si) piezoresistive beams, with two pairs of sidewall-doped Si beams for shear stress sensing and one pair of surface-doped Si beams for normal stress sensing[24]. However, the sensing component is not durable, as Si is mechanically brittle and cannot withstand large deformations[25]. Mo *et al.* presented a tactile sensor integrated with a thin-film-based piezoresistive array for tri-axial force measurement[26]. As the sensor uses a rigid substrate and has a large overall size, it can hardly be used in robotic arms or hands. Flexible tactile sensors that can perform multi-directional sensing are highly demanded in robotic systems. To meet the need for flexible tactile sensors, Sun *et al.* reported a flexible electronic skin based on carbon nanotube (CNT)/polydimethylsiloxane (PDMS) nanocomposites for tri-axial contact force detection[27]. Choi developed a flexible tri-axial tactile sensor using polymer micromachining technology[28]. Although these flexible tactile sensors are sensitive to muti-directional forces, decoupling these forces with high linearity remains a great challenge.

In this paper, we propose a flexible tactile sensor with a novel embedded-hair-in-elastomer (EHiE) structure, which can decouple normal stress and shear stress. The tactile sensor adopts polyimide (PI) as the substrate and self-bending piezoresistive cantilevers in a cross-shaped configuration as the sensing component. The sensing principle of the sensor for normal and shear stresses is proposed and verified from simulations and experiments, respectively. The flexible sensor can decouple the tri-axial stress with simple summation and differencing algorithms. The flexible nature of the sensor makes it appropriate for both conventional robotic arms with curved surfaces and soft robotic grippers.

RESULTS AND DISCUSSION

Design and principle

The design of the flexible tactile sensor is illustrated in Figure 1A. The tactile sensor consists of four curved cantilevers arranged in a cross-shaped configuration embedded in an elastomer. Platinum (Pt) piezoresistors patterned in a serpentine shape are located at the root of the curved cantilevers. As the tactile sensor is fabricated on a flexible PI substrate[29], it can be placed on arbitrarily shaped surfaces for the detection of normal stress and shear stress. When the tactile sensor is subjected to an external force, the elastomer deforms, and the cantilevers embedded in the elastomer follow the deformation.

A theoretical model is developed based on the design dimensions of the sensor, as shown in Figure 1B and C. The resistance changes of the piezoresistors can be estimated when the shear and normal stresses are applied to the sensor. The following assumptions are made in this model[30]: (1) the presence of the flexible cantilevers does not affect the deformation of the elastomer; (2) the cantilevers follow the deformation of the elastomer completely; (3) the stresses applied to the sensor are small.

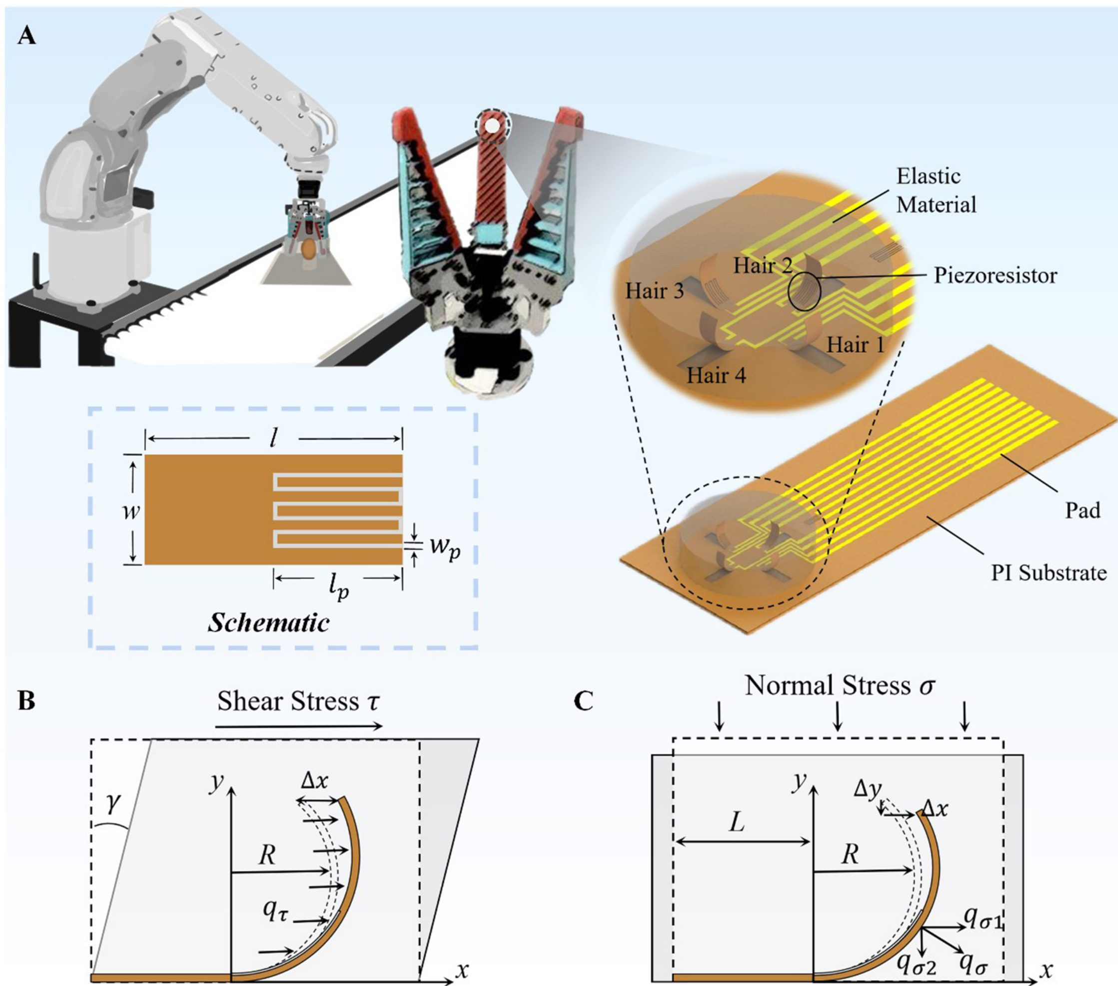

Figure 1. Schematic of the flexible tactile sensor. (A) Concept of the tactile sensor. Curved piezoresistive cantilevers in a cross-shaped configuration embedded in an elastomer for normal stress and shear stress sensing; (B) Deformation of cantilevers of the tactile sensor under shear stress; (C) Deformation of cantilevers under normal stress. PI: Polyimide.

As shown in Figure 1B, the deformation Δx at the free end of the curved cantilever for a shear stress τ is given by:

$$\Delta x = \gamma \cdot y = \frac{\tau}{G} \cdot \frac{3}{2} R \quad (1)$$

where G is the shear modulus of the elastic material, and R is the radius of the curved cantilever. The cantilever beam has a circular angle of approximately 120°, and the length of the piezoresistor is half of the cantilever length. According to the model, uniform force q_τ is applied to the cantilever. According to Equation (1), the stress σ_τ occurs along the length of the cantilever, which can be calculated as:

$$\sigma_\tau = \frac{M(y)}{W_z} = \frac{3q_\tau(\frac{3}{2}R - y)^2}{wt^2} \tag{2}$$

The resistance of the piezoresistor changes linearly with its deformation in the longitudinal direction. According to Equation (2), the change in resistance of the piezoresistor is calculated as:

$$\frac{\Delta R}{R} = \pi_l \int_0^{\frac{1}{2}R} \sigma_\tau dy \tag{3}$$

$$q_\tau = k_x \cdot \Delta x \tag{4}$$

where π_l is the piezoresistive coefficient in the longitudinal direction, and k_x is the spring constant of the cantilever in the X direction. By combining Equations (1)-(4), the fractional change in resistance of the piezoresistor can be calculated as Equation (5).

$$\frac{\Delta R}{R} = \frac{57}{16}\frac{\pi_l}{wt^2}k_x R^4 \frac{\tau}{G} = D_\tau \tau \tag{5}$$

Where D_τ is a constant that shows the relationship between the fractional change in resistance and the applied shear stress.

Similarly, as shown in Figure 1C, the deformation at the free end of the curved cantilever for the normal stress σ is given by:

$$\Delta y = \frac{\sigma}{E} \cdot y = \frac{\sigma}{E} \cdot \frac{3}{2}R \tag{6}$$

$$\Delta x = \mu\frac{\sigma}{E} \cdot x = \mu\frac{\sigma}{E}\left(L + \frac{\sqrt{3}}{2}R\right) \tag{7}$$

where E is the Young's modulus of the elastic material, and L is the distance from the root of the cantilever to the central axis of the elastomer cap. According to the model, uniform force q_σ is applied to the cantilever and can be decomposed into two components. The stresses generated by these two force components applied to the cantilever are calculated as:

$$\sigma_{\sigma 1} = \frac{M(y)}{W_z} = \frac{3q_{\sigma 1}(\frac{3}{2}R - y)^2}{wt^2} \tag{8}$$

$$\sigma_{\sigma 2} = \frac{M(x)}{W_z} = \frac{6q_{\sigma 2}\left(R - \frac{\sqrt{3}}{2}R\right)\left(R + \frac{\sqrt{3}}{2}R - 2x\right) + 3q_{\sigma 2}(\frac{\sqrt{3}}{2}R - x)^2}{wt^2} \tag{9}$$

When the normal stress is applied, the fractional change in resistance is given by:

$$\frac{\Delta R}{R} = \pi_l\left(\int_0^{\frac{1}{2}R} \sigma_{\sigma 1} dy + \int_0^{\frac{\sqrt{3}}{2}R} \sigma_{\sigma 2} dx\right) \tag{10}$$

$$q_{\sigma 1} = k_x \cdot \Delta x \tag{11}$$

$$q_{\sigma 2} = k_y \cdot \Delta y \tag{12}$$

According to Equations (6)-(12), the fractional change in resistance to the normal stress is expressed as:

$$\frac{\Delta R}{R} = \frac{\pi_l}{wt^2}\left[\frac{45\sqrt{3} - 54}{8} k_y R^4 + \frac{19}{8} \mu k_x R^3 \left(L + \frac{\sqrt{3}}{2}R\right)\right]\frac{\sigma}{E} = D_\sigma \sigma \tag{13}$$

where D_σ is a constant that shows the relationship between the fractional change in resistance and the applied normal stress.

According to Equations (5) and (13), when both normal stress and shear stress are applied, the change in resistance of the piezoresistor is given by:

$$\frac{\Delta R}{R} = D_\tau \tau + D_\sigma \sigma \tag{14}$$

Equation (14) shows that the resistance of the tactile sensor changes linearly with the applied normal stress and shear stress, respectively.

3D solid mechanics simulation was performed to illustrate the deformation of the EHiE structure and the strain distribution along the cantilevers when the normal stress and shear stress were applied. The dimensions of the tactile sensor are listed in Table 1[31]. As shown in Figure 2A, the hair-like cantilever deforms with the elastomer when a uniform stress is applied to the elastomer surface. The average strain at the location of the piezoresistor on the hair-like cantilever is extracted to calculate the resistance change of

Cao *et al. Soft Sci* 2023;3:32 | https://dx.doi.org/10.20517/ss.2023.22

Table 1. Design dimensions for the tactile sensor

	Cantilever	Pt piezoresistor
Length	l = 1.5 mm	l_p = 0.75 mm
Width	w = 0.5 mm	w_p = 20 μm
Thickness	t = 9 μm	t_p = 30 nm
Number of serpentine turns		6

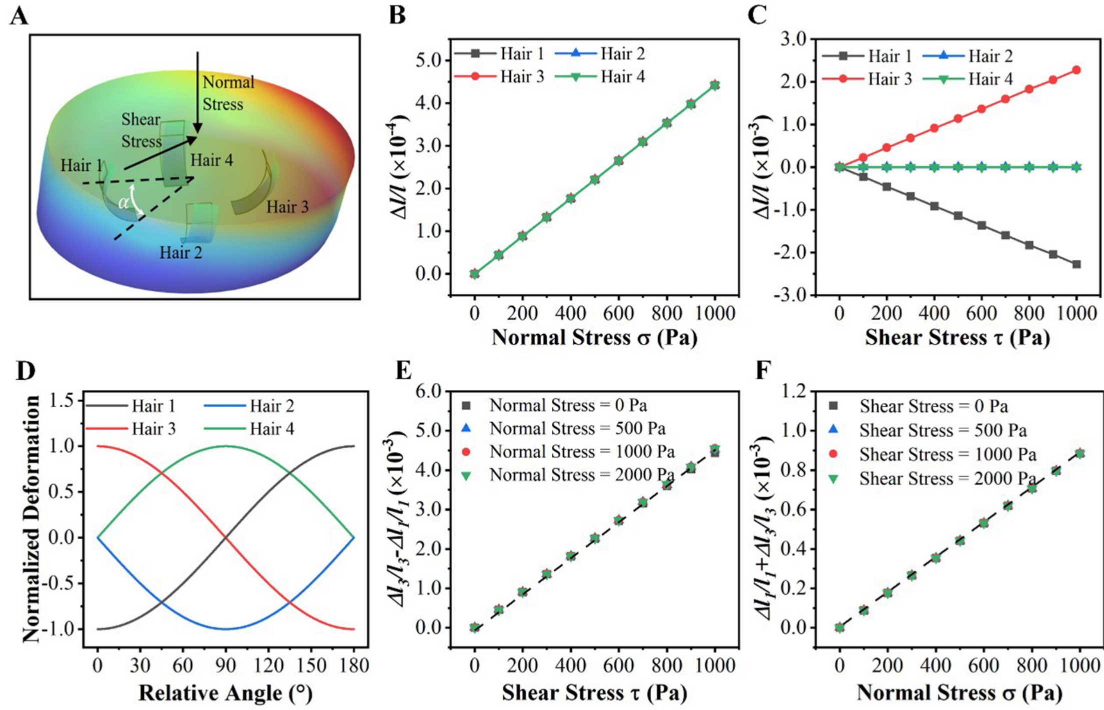

Figure 2. 3D solid mechanics simulation results of the tactile sensor. (A) Deformation of the tactile sensor when normal stress and shear stress are applied; (B) Normal stress and (C) shear stress induced average strains of four cantilevers where the piezoresistors are located; (D) Normalized deformation of the four cantilevers when the angle of shear stress changes from 0° to 180°; (E) Differencing and (F) summation results of the average strains of Hair 1 and Hair 3 when both normal stress and shear stress are applied.

the piezoresistor. The resistance change (ΔR) as a function of the average strain ($\bar{\varepsilon}$) can be written as

$$\Delta R = GF \cdot \bar{\varepsilon} R_0 \tag{15}$$

where GF is the gauge factor of the piezoresistor.

As shown in Figure 2B, the average strains of four hair-like cantilevers (Hair 1-4) are identical and linearly related to the magnitude of the normal stress. As shown in Figure 2C, when a shear stress with a position angle (α) of 0° is applied, the average strains of two hair-like cantilevers (Hair 1 and Hair 3) that are in the direction of the shear stress show a linear relationship with the magnitude of the shear stress, while the average strains of the other two hair-like cantilevers (Hair 2 and Hair 4) are essentially unchanged. It indicates that the hair-like cantilevers can detect the component of shear stress vertical to their surfaces. Figure 2D shows the normalized results of the average strains of the four hair-like cantilevers when the

direction of the shear stress is gradually rotated from 0° to 180°. It can be noticed that the average strain reaches a maximum value when the angle between the shear stress and the hair-like cantilever beam is 0° and 180° and decreases to zero when the angle between the shear stress and the hair-like cantilever is ±90°. The normalized deformation of the four hair-like cantilevers produced a phase difference of 90°, confirming the capability of the tactile sensor for omnidirectional detection of the shear stress.

When a normal stress and a shear stress ($\alpha = 0°$) are applied concurrently, the average strain due to the normal stress can be eliminated by differencing the average strains of Hair 1 and Hair 3 according to Equation (14). As shown in Figure 2E, the results obtained from the average strain difference between Hair 1 and Hair 3 are linearly related to the magnitude of the shear stress, which is valid for different normal stress conditions. Similarly, the average strain due to the shear stress can be eliminated by summing the average strains of Hair 1 and Hair 3. As shown in Figure 2F, the summation of the average strains of Hair 1 and Hair 3 is proportional to the magnitude of the normal stress. Moreover, its sensitivity to normal stress is consistent at different shear stress conditions.

Based on the above analysis, the output of the tactile sensor can be decoupled to obtain specific values of normal and shear stresses. Assuming that the direction of the shear stress is 0° to Hair 1 and Hair 3, the specific decoupling process consists of the following two steps: (1) The outputs of Hair 1 and Hair 3 are differenced, and the applied shear stress can be obtained by comparing the differencing result with calibrated shear stress sensitivity; (2) The outputs of Hair 1 and Hair 3 are summed, and the applied normal stress can be obtained by comparing the summation result with the calibrated normal stress sensitivity.

Fabrication

Figure 3 illustrates the fabrication process of the flexible tactile sensor[31]. A single-polished Si wafer is used as the substrate [Figure 3A]. PI resist is spin-coated on the Si substrate and cured by gradient heating to form the PI film, which is used as the substrate of the flexible tactile sensor [Figure 3B]. Sputtering and lift-off processes are used to form a 500 nm thick, 1.6 mm long, and 0.6 mm wide Cu sacrificial layer [Figure 3C]. A similar process is used to form a 200 nm thick, 1.5 nm long, and 0.5 mm wide Si layer [Figure 3D]. Another layer of PI film with a thickness of 10 μm is formed by spin-coating and curing [Figure 3E]. Then, a Pt layer with a thickness of 30 nm is patterned on the second PI film to form the piezoresistors [Figure 3F]. Similarly, Au electrodes with a thickness of 300 nm are formed for electrical connections [Figure 3G]. After photolithography, reaction ion etching (RIE) is used to define the structure of the cantilevers and expose the Cu sacrificial layer [Figure 3H]. The Cu sacrificial layer is etched using $FeCl_3$ solution (10 *wt*%), and the photoresist is removed. Due to the difference in thermal expansion coefficients between Si and PI, the stress difference between the Si and Pi layers leads to the self-bending of the cantilever, forming a 3D curved hair-like structure [Figure 3I]. Finally, a mold is used to cast and cure the elastic material to form the EHiE structure of the tactile sensor [Figure 3J].

Characterization of the tactile sensor

The fabrication result of the flexible tactile sensor is shown in Figure 4A. The electrodes and piezoresistors of the sensor are well patterned. The cantilevers arranged in a cross-shaped configuration show a well-formed bending curvature and consistency. The tactile sensor encapsulated with elastic material is shown in Figure 4B. The elastomer cap with a diameter of 6 mm and a thickness of 1 mm completely covers the four piezoresistive cantilevers and is tightly bonded to the PI substrate. The relatively fragile sensitive components of the sensor are completely encapsulated in an elastomer, which not only improves the service life of the sensor but also provides excellent environmental resistance and allows it to function properly even when it comes into contact with water or dust. The experimental setup of the tactile sensor is shown in Figure 4C. A micro-motion platform with a displacement resolution of 0.1 μm was used to apply normal

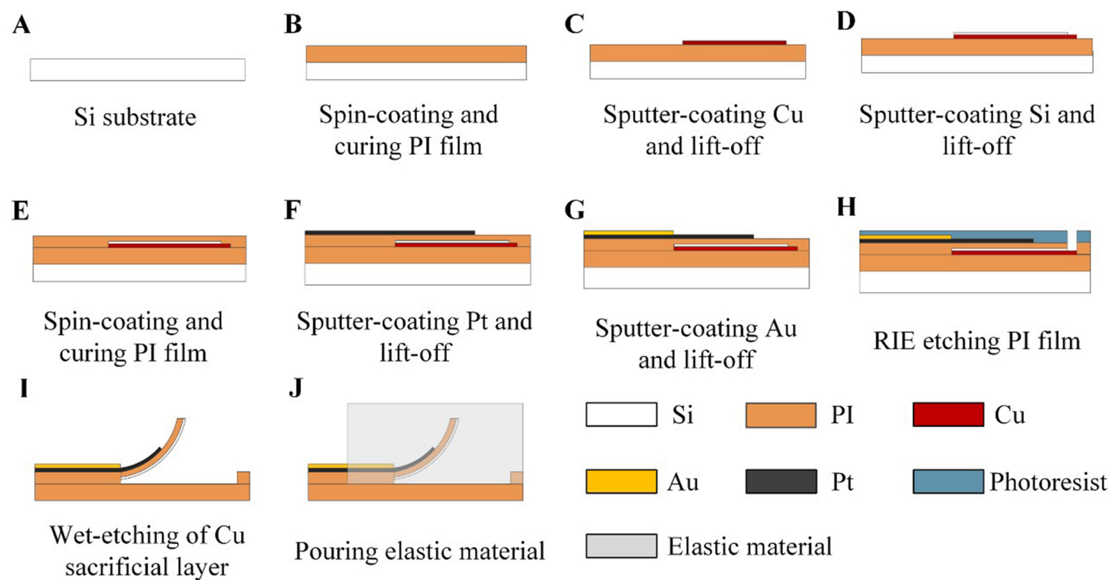

Figure 3. Fabrication of the flexible tactile sensor. (A) Preparation of the Si substrate; (B) Spin-coating and curing PI film; (C) Sputtering and lift-off of a Cu sacrificial layer; (D) Sputtering and lift-off of a Si layer; (E) Spin-coating and curing a second layer of PI film (10 μm); (F) Sputtering and lift-off of Pt piezoresistors; (G) Sputtering and lift-off Au electrodes; (H) RIE of PI; (I) Removing the Cu sacrificial layer; (J) Pouring and curing of an elastomer. PI: Polyimide; RIE: reaction ion etching; Si: silicon.

and shear stresses to the tactile sensor. Two force transducers (LH-75-50, Liheng Sensors Co., Ltd.) were used to calibrate the normal and shear stresses. The resistance outputs of the piezoresistors in the tactile sensor were simultaneously measured by a multi-channel SourceMeter (DAQ6510, Tektronix Co., Ltd.).

Figure 4D shows the fractional change in resistance of each cantilever as a function of the normal stress. The four cantilevers deformed in the same way as the elastomer when the tactile sensor is subjected to downward normal stress. In the range of 0-2.0 kPa, the fractional change in resistance of the piezoresistors is proportional to the magnitude of the normal stress, and the sensitivity shows good consistency. The sensitivity of Hair 1 is 3.74×10^{-7} Pa^{-1}, and the detection threshold of normal stress is approximately 13.7 Pa as the root mean square (RMS) of noise is 5.14×10^{-6}. The four piezoresistive cantilevers of the sensor have similar outputs for normal stress. The normal stress detection threshold is reduced to 7.2 Pa by simply summing the outputs of the four cantilevers to improve the signal-to-noise ratio.

Figure 4E shows the fractional change in resistance of each cantilever as a function of the shear stress. Hair 1 and Hair 2 are two curved cantilevers arranged in the orthogonal direction. When shear stress with a position angle of 0° to Hair 1 is applied, the piezoresistor on the surface of Hair 1 is subjected to compressive stress, resulting in a decrease in resistance. On the contrary, when a shear stress with a position angle of 180° to Hair 1 is applied, the piezoresistor on the surface of Hair 1 is subjected to tensile stress, resulting in an increase in resistance. In the range of -1.3 to 2.0 kPa, the resistance of the piezoresistor of Hair 1 varies linearly with the magnitude of the applied shear stress. The shear stress sensitivity of Hair 1 is 7.91×10^{-7} Pa^{-1}, and the detection threshold is 6.9 Pa. As Hair 1 and Hair 3 are both sensitive to the shear stress in opposite directions, the shear stress detection threshold can be reduced to 5.1 Pa by differencing the outputs of Hair 1 and Hair 3.

The fractional change in resistance of the piezoresistor changes with the direction of the shear stress, as shown in Figure 4F. The magnitude of the shear stress is held constant at 3.5 kPa, and the direction of the

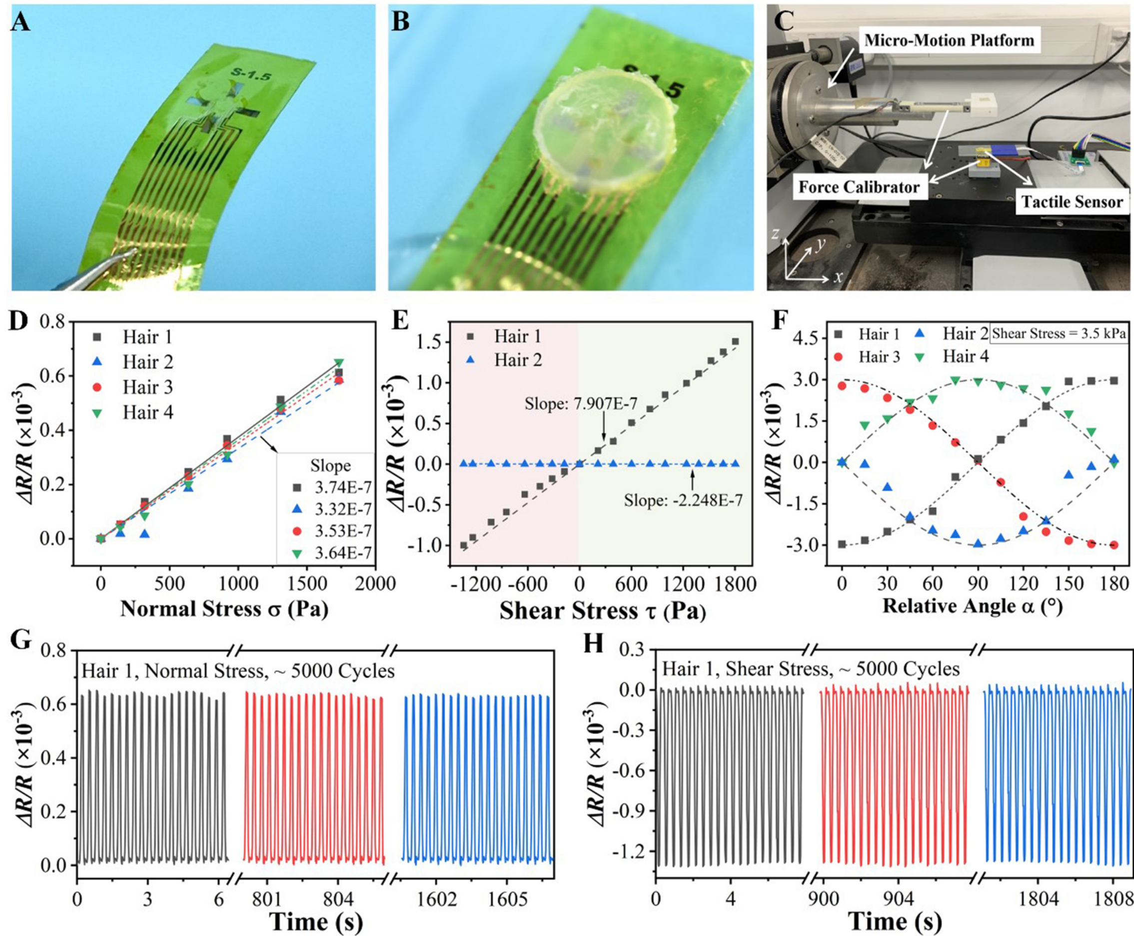

Figure 4. Characterization of the flexible tactile sensor. (A) Fabrication result of self-bending piezoresistive cantilevers; (B) Tactile sensor with the EHiE structure; (C) Experimental setup for tactile testing; (D) Fractional change in resistance variation with normal stress; (D) Fractional change in resistance variation with shear stress; (F) Fractional change in resistance when varying the direction of shear stress; (G) Good repeatability and durability after continuous about 5,000 normal stress loading-unloading cycles; (H) Good repeatability and durability after continuous about 5,000 shear stress loading-unloading cycles. EHiE: Embedded-hair-in-elastomer.

shear stress is varied from 0° to 180° with a step of 30°. The four cantilevers show a consistent sinusoidal response to the direction change of the shear stress, which indicates that the sensor can potentially detect omnidirectional shear stress.

In order to test the dynamic stability performance of the sensor, about 5,000 continuous normal stress and shear stress loading–unloading cycles have been applied to the tactile sensor, respectively. Dynamic resistance responses of the piezoresistor of Hair 1 are depicted in Figure 4G and H. We can see that the sensor shows good stability and repeatability, which are important for tactile sensing applications. In addition, the sensor perfectly follows the motion of the force applicator during the stress loading-unloading cycles of 3~4 Hz, which indicates that the tactile sensor has a good recovery rate.

Decoupling of normal stress and shear stress

By analyzing the outputs of the piezoresistors, we can obtain the magnitudes of the normal stress and shear stress. This section will verify the decoupling mechanism experimentally. Firstly, the piezoresistive outputs of Hair 1 and Hair 3 need to be differenced (referred to as *DIFF result*) to eliminate the effect of the normal

stress. There are two prerequisites for implementing Step 1. The first one is that Hair 1 and Hair 3 have the same sensitivity to normal stress. Figure 4D shows the good sensitivity consistency of the four cantilevers for the normal stress. The second one is the consistent sensitivity of the *DIFF result* to shear stress at different normal stress conditions. Figure 5A shows that the *DIFF results* are linearly related to the applied shear stress with good consistency of sensitivity in the range of 0-2,000 Pa when normal stresses of 0, 693, and 1,925 Pa are applied, respectively. Therefore, the mean value of the slopes of the fitted lines in Figure 5A is taken as the calibrated shear stress sensitivity, and the shear stress calculated by the *DIFF result* is kept within 3.0% error from the actual applied shear stress.

After determining the magnitude of the shear stress, the resistance changes of Hair 1 and Hair 3 are summed (referred to as the *SUM result*) to estimate the normal stress by eliminating the influence of the shear stress. It should be noted that the *SUM result* cannot completely eliminate the influence of the shear stress, as shown in Figure 5B, due to unavoidable manufacturing errors and structural asymmetry of the self-bending cantilevers. However, the initial value of the *SUM result* when no normal stress is applied can be obtained by comparing the shear stress obtained in Step 1. We can still solve the normal stress combined with the shear stress, provided that the sensitivity of the *SUM result* to the normal stress remains consistent under different shear stress conditions. Figure 5C shows the response of the *SUM result* to the normal stress for different shear stresses applied. When shear stresses of 0, 693, 1,039, and 1,733 Pa are applied, respectively, the *SUM results* are linear with respect to the normal stress with good consistency of sensitivity. The mean value of the slopes of the fitted lines is taken as calibrated normal stress sensitivity. The *SUM Results* of the four experimental results at the normal stress of 0 (i.e., intercepts) are extracted and labeled in the fitted lines in Figure 5B (marked with red stars). As expected, the four initial values highly comply with the *SUM result* in Figure 5B. Therefore, the intercept and slope can be determined in the step of solving the shear stress, and then the magnitude of the normal stress can be calculated from the *SUM result*. The experiment result indicates that the calculation error of the normal stress is within 2.9%. Table 2 displays the comparison of this work with recently reported tactile sensors based on different sensing principles, which indicates the outstanding comprehensive performance, such as sensitivity and dimension, of the proposed fully flexible tactile sensor. Based on this, there are some potential methods that can improve the sensitivity performance of the sensor. The sensitivity of the proposed EHiE structure of the tactile sensor is related to the Young's modulus of the elastomer; thus, a softer elastic material can be selected to enhance the sensitivity of the sensor. In addition, the choice of piezoresistive material with a larger *GF* to be used as the sensitive component of the sensor is also one of the ways to improve the performance of the sensor.

Variable sensitivity of the tactile sensor

It is highly desirable that the sensitivity and detection threshold of the tactile sensor can be modified for a broad area of applications. Here, we propose a simple method to change the sensitivity of the sensor by changing the elastic material. According to Equations (5) and (13), the sensitivity of the sensor to both shear stress and normal stress is inversely proportional to Young's modulus of the elastic material. The larger the Young's modulus of the elastic material, the lower the sensitivity of the sensor, or vice versa. Figure 6A and B shows the response of the tactile sensor to normal and shear stresses when PDMS and hydrogel are adopted as the elastic material, respectively. The sensor output remains linearly related to the magnitude of normal stress and shear stress. However, since Young's modulus of PDMS and hydrogel are 750 kPa and 150 kPa, respectively, the sensitivity of the sensor using PDMS as the elastic material is much lower than that of the sensor using hydrogel as the elastic material. Figure 6C shows the sensitivities of the sensors adopting PDMS, Ecoflex, and hydrogel as the elastic material, respectively. As expected, the sensitivity of the sensor to both normal stress and shear stress is inversely proportional to Young's modulus of the elastic material. This simple sensitivity modification method can endow the tactile sensor with an enhanced sensitivity or a wide detection range.

Table 2. Performance of relevant tactile sensors reported recently

Author	Sensing principle	Normal stress sensitivity	Shear stress sensitivity	Dimensions (mm)
Lee *et al.*[6]	Piezoresistive	2.1×10^{-4} (kPa^{-1})	5.9×10^{-5} (kPa^{-1})	4.2 (*l*) × 2.9 (*w*) × 0.25 (*t*)
Takahashi *et al.*[24]	Piezoresistive	1.3×10^{-5} (kPa^{-1})	4.6×10^{-5} (kPa^{-1})	10 (*l*) × 10 (*w*) × 10 (*t*)
Noda *et al.*[17]	Capacitive	7.4×10^{-4} (kPa^{-1})	3.2×10^{-4} (kPa^{-1})	35 (*l*) × 35 (*w*) × 2.1 (*t*)
Dobrzynska *et al.*[15]	Capacitive	6.6×10^{-4} (kPa^{-1})	2.8×10^{-4} (kPa^{-1})	10 (*l*) × 10 (*w*)
This work	Piezoresistive	7.1×10^{-4} (kPa^{-1})	1.5×10^{-3} (kPa^{-1})	6 (*d*) × 1 (*t*)

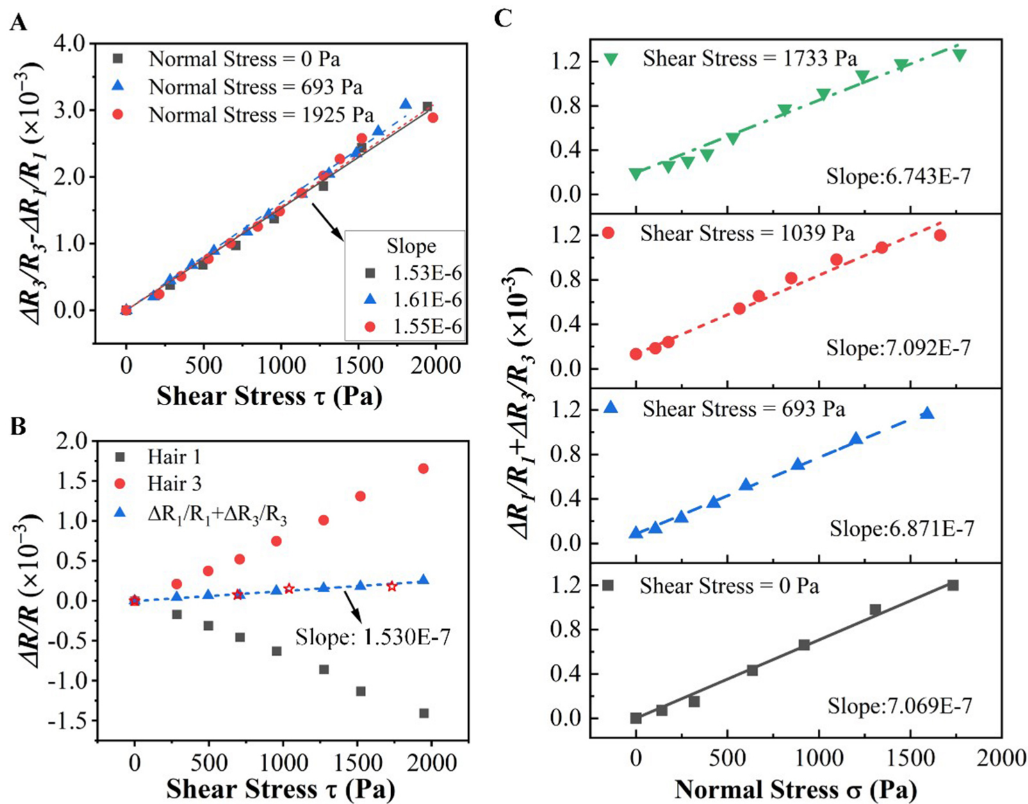

Figure 5. Stress decoupling results. (A) *DIFF results* of Hair 1 and Hair 3 to the shear stress when normal stresses of 0, 693, and 1,925 Pa are applied, respectively; (B) Resistance changes of Hair 1, Hair 3 and the *SUM result* to the shear stress; (C) *SUM results* of Hair 1 and Hair 3 to the normal stress when shear stresses of 0, 693, 1,039, and 1,733 Pa are applied, respectively.

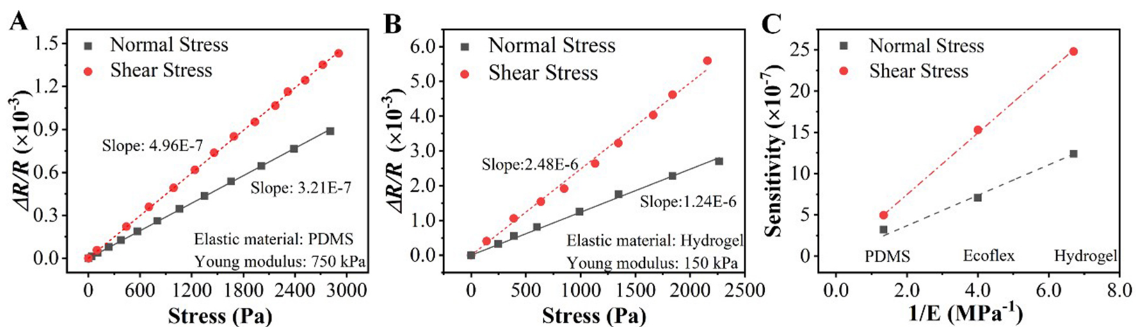

Figure 6. Variable sensitivity of tactile sensors. Response of the sensor to normal stress and shear stress when (A) PDMS and (B) hydrogel are adopted as elastic materials, respectively; (C) Sensor sensitivity as a function of Young's modulus of elastic material.

Cao *et al. Soft Sci* 2023;3:32 | https://dx.doi.org/10.20517/ss.2023.22

Application in robotic grasping operation

To operate in changing environments, robots need to sense and elaborate the information about the surrounding environment while interacting with real-world objects. It is demonstrated here that the proposed fully flexible tactile sensors can be perfectly integrated into a robot system and sense the gripping force of the manipulator and weight of grasped objects in real time, which proves its great potential for application in a robot system. Figure 7A shows the soft manipulator integrated with the tactile sensor. The soft manipulator was mounted on a desktop robot to realize the grasping operation of objects, and the desktop robot can freely translate in the *XYZ* direction to locate the object. The tactile sensor was mounted on one of the jaws of the manipulator, and the weight of the grasped object can be obtained by the normal stress and shear stress measured by the tactile sensor.

In this demonstration, four objects are used for classification, three of which are eggs, and the other is a plastic ball with a small weight. The actual weight of the objects is shown in Table 3. The grasping action is divided into three detailed steps: free, clamping, and lifting. In the free state, there is no contact between the manipulator and the object. In the clamping state, the object is subjected to clamping forces from the three directions of the manipulator, which are the normal stress measured by the tactile sensor. In the lifting state, on the basis of step 2, the object is subjected to the static friction forces of the three jaws of the manipulator and balanced with its gravity. When the manipulator lifts the object, the shear stress applied to the tactile sensor can be expressed as: $\tau_t = f/A$, where f and A are the static friction force and the contact area between the object and the sensor, respectively. Therefore, the shear stress applied to the sensor is proportional to the static friction force and the weight of the object.

Figure 7B shows the *DIFF result* between the two cantilevers of the tactile sensor in relation to the shear stress applied to the sensor when lifting the object. The sensor output is proportional to the magnitude of the shear stress, and the sensitivity to shear stress is 1.55×10^{-6} Pa^{-1}. It indicates that the weight of the grasped object can be estimated by measuring the shear stress to complete the classification of the object.

Figure 7C shows the fractional change in resistance of the tactile sensor during the object grasping operation. In the free state, the sensor is not subjected to force, and the resistance of piezoresistors remains unchanged. In the clamping state, the sensor is subjected to normal stress, and the resistance increases, and the *SUM result* is linearly related to the magnitude of the clamping force. In the lifting state, as the sensor is subjected to both normal and shear stresses, one of the cantilever resistances decreases, and the other cantilever resistance increases. Figure 7D shows the *DIFF* and *SUM results* of the two cantilevers of the tactile sensor in the three states. The normal stress increases in the clamping state, and then the *DIFF result* shows an increase in the shear stress in the lifting state.

CONCLUSIONS

Tactile sensors play an important role in robotic systems to interact safely and intelligently with humans and environments. In this study, a novel EHiE structure-based flexible tactile sensor is proposed for the detection of normal stress and shear stress. Experimental results show that the response of the proposed tactile sensor is proportional to the magnitudes of the applied stress, and the detection thresholds can reach 7.2 Pa and 5.1 Pa for normal stress and shear stress, respectively. In addition, for touch-induced stress with an unknown direction, it can be decoupled into the corresponding normal stress and shear stress, and the measurement error is kept within 3%. As the tactile sensor is flexible, highly sensitive, and capable of detecting both normal stress and shear stress, it shows great potential for applications in the field of Tri-Co Robots.

Table 3. Weight of the grasped objects in the robot grasping experiment

Object No.	Object category	Weight (mN)
1	Egg	502.4
2	Egg	558.0
3	Egg	623.7
4	Plastic ball	135.6

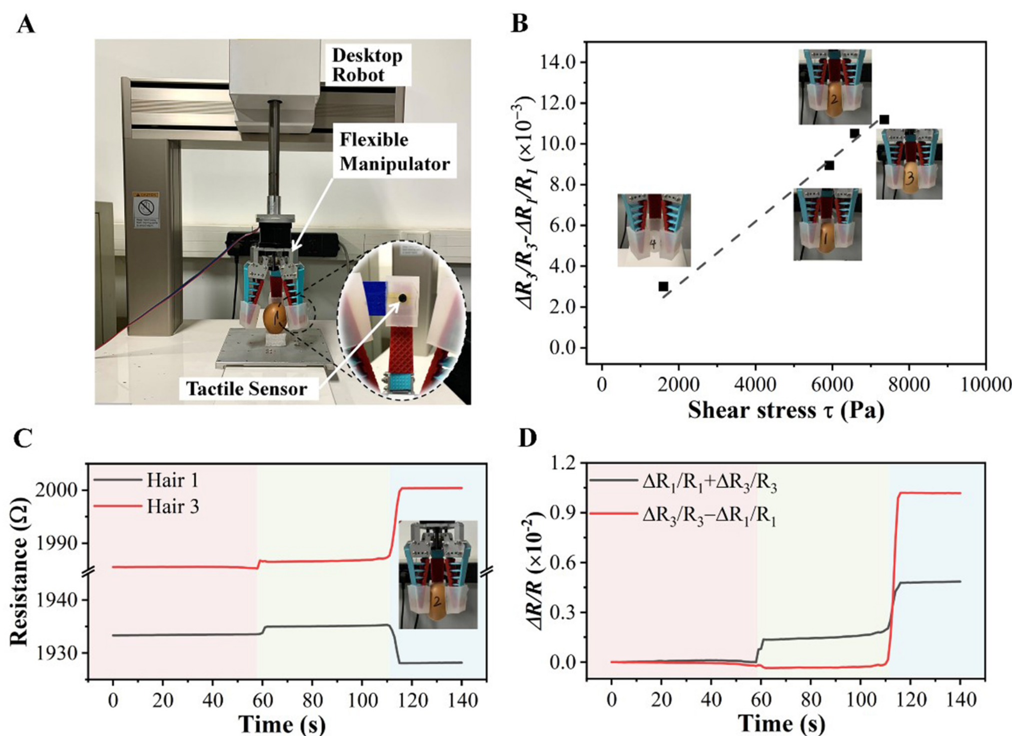

Figure 7. Demonstration of the tactile sensor in robotic grasping operation. (A) Experimental setup for robotic grasping; (B) The *DIFF result* of Hair 1 and Hair 3 when lifting the objects; (C) Resistance changes of Hair 1 and Hair 3 when grasping the object 2; (D) *SUM* and *DIFF results* of Hair 1 and Hair 3 when grasping the object 2.

METHOD

Configuration of 3D solid mechanics simulation

The COMSOL Multiphysics simulation software was used to analyze the proposed sensor. Firstly, a 3D model of the sensor was created in the modeling software SolidWorks and imported into COMSOL. Then, the component materials were defined, with PI (E = 3.2 GPa, μ = 0.34) as the material for the four cantilevers in a cross-shaped configuration and PDMS (E = 750 kPa, μ = 0.49) as the elastomer material. A fixed constraint was applied to the bottom surface of the elastomer, and stresses were applied to the top surface of the elastomer using the boundary load method. A free tetrahedral mesh was used, and the mesh cell size was adjusted appropriately. After completing the above configuration, calculations were performed, and the average strain of the piezoresistive structure was extracted as the resulting output.

Preparation of elastic material

Three elastic materials were used in the fabrication of the proposed tactile sensors: PDMS, Ecoflex, and hydrogel. PDMS is a silicone material that employs the 184 Silicone Elastomer Kit produced by SYLGAND. The basic component and the curing agent were mixed completely in a 10:1 weight ratio and cured at a temperature range of 25 to 150 °C. After completely curing, the Young's modulus of PDMS is

approximately 750 kPa. Ecoflex is a Pt-catalyzed silicone that employs Ecoflex™ produced by SMOOTH-ON. Ecoflex was mixed 1A:1B by weight and cured at a temperature range of 30 to 90 °C. After completely curing, the Young's modulus of Ecoflex was approximately 250 kPa. For the hydrogel, 5 g of acrylamide (AAM, Macklin Co., Ltd.), 0.03 g of poly (ethylene glycol) diacrylate (PEGDA, Macklin Co., Ltd.), and 0.25 g of 2,4,6-trimethylbenzoyldiphenyl phosphine oxide (TPO, Macklin Co., Ltd.) were dissolved in 15.6 g of deionized water. The mixture was formed into a hydrogel using a light-curing method. The Young's modulus of the hydrogel was approximately 150 kPa.

DECLARATIONS

Authors' contributions

Conceptualization: Jiang Y, Zhang D, Cai J
Methodology: Cao Y, Li J, Jiang Y
Formal analysis: Cao Y
Software: Cao Y, Dong Z, Sheng T
Writing - original draft preparation: Cao Y
Writing - review and editing: Cao Y, Jiang Y

Availability of data and materials

The data presented in this study are available on request from the corresponding author.

Financial support and sponsorship

This work is supported by the Beijing Municipal Natural Science Foundation (M22021) and partly supported by the National Natural Science Foundation of China (Nos. 52022008, 51975030, T2121003).

Conflicts of interest

All authors declared that there are no conflicts of interest.

Ethical approval and consent to participate

Not applicable.

Consent for publication

Not applicable.

Copyright

© The Author(s) 2023.

REFERENCES

1. Ding H, Yang X, Zheng N, Li M, Lai Y, Wu H. Tri-Co Robot: a Chinese robotic research initiative for enhanced robot interaction capabilities. *Natl Sci Rev* 2018;5:799-801. DOI
2. Stassi S, Cauda V, Canavese G, Pirri CF. Flexible tactile sensing based on piezoresistive composites: a review. *Sensors* 2014;14:5296-332. DOI PubMed PMC
3. Bartolozzi C, Natale L, Nori F, Metta G. Robots with a sense of touch. *Nat Mater* 2016;15:921-5. DOI PubMed
4. Mahmud MAP, Bazaz SR, Dabiri S, et al. Advances in MEMS and microfluidics-based energy harvesting technologies. *Adv Mater Technol* 2022;7:2101347. DOI
5. Tang D, Abdalkarim SYH, Dong Y, Yu HY. One-pot strategy to fabricate conductive cellulose nanocrystal-polyethylenedioxythiophene nanocomposite: synthesis mechanism, modulated morphologies and sensor assembly. *Carbohydr Polym* 2023;311:120758. DOI
6. Lee JI, Kim MG, Shikida M, Sato K. A table-shaped tactile sensor for detecting triaxial force on the basis of strain distribution. *Sensors* 2013;13:16347-59. DOI PubMed PMC
7. Thanh-Vinh N, Binh-Khiem N, Matsumoto K, Shimoyama I. High sensitive 3D tactile sensor with the structure of elastic pyramids on piezoresistive cantilevers. In: 2013 IEEE 26th International Conference on Micro Electro Mechanical Systems (MEMS); Taipei,

China. IEEE; 2013. p. 41-4. DOI
8. Wang Y, Wu X, Mei D, Zhu L, Chen J. Flexible tactile sensor array for distributed tactile sensing and slip detection in robotic hand grasping. *Sens Actuator A Phys* 2019;297:111512. DOI
9. Cao M, Su J, Fan S, Qiu H, Su D, Li L. Wearable piezoresistive pressure sensors based on 3D graphene. *Chem Eng J* 2021;406:126777. DOI
10. Dahiya RS, Metta G, Valle M, Adami A, Lorenzelli L. Piezoelectric oxide semiconductor field effect transistor touch sensing devices. *Appl Phys Lett* 2009;95:034105. DOI
11. Chuang CH, Wang MS, Yu YC, Mu CL, Lu KF, Lin CT. Flexible tactile sensor for the grasping control of robot fingers. In: 2013 International Conference on Advanced Robotics and Intelligent Systems; Tainan, China. IEEE; 2013. p. 141-6. DOI
12. Park SH, Lee HB, Yeon SM, Park J, Lee NK. Flexible and stretchable piezoelectric sensor with thickness-tunable configuration of electrospun nanofiber mat and elastomeric substrates. *ACS Appl Mater Interfaces* 2016;8:24773-81. DOI
13. Jiang Y, Ma Z, Cao B, Gong L, Feng L, Zhang D. Development of a tactile and slip sensor with a biomimetic structure-enhanced sensing mechanism. *J Bionic Eng* 2019;16:47-55. DOI
14. Surapaneni R, Guo Q, Xie Y, Young DJ, Mastrangelo CH. A three-axis high-resolution capacitive tactile imager system based on floating comb electrodes. *J Micromech Microeng* 2013;23:075004. DOI
15. Dobrzynska JA, Gijs MAM. Polymer-based flexible capacitive sensor for three-axial force measurements. *J Micromech Microeng* 2013;23:015009. DOI
16. Liang G, Mei D, Wang Y, Chen Z. Modeling and analysis of a flexible capacitive tactile sensor array for normal force measurement. *IEEE Sensors J* 2014;14:4095-103. DOI
17. Noda K, Matsumoto K, Shimoyama I. Stretchable tri-axis force sensor using conductive liquid. *Sens Actuator A Phys* 2014;215:123-9. DOI
18. Takenawa S. A soft three-axis tactile sensor based on electromagnetic induction. In: 2009 IEEE International Conference on Mechatronics; Malaga, Spain. IEEE; 2009. p. 1-6. DOI
19. Kawasetsu T, Horii T, Ishihara H, Asada M. Flexible tri-axis tactile sensor using spiral inductor and magnetorheological elastomer. *IEEE Sensors J* 2018;18:5834-41. DOI
20. Wang H, Kow J, Raske N, et al. Robust and high-performance soft inductive tactile sensors based on the Eddy-current effect. *Sens Actuator A Phys* 2018;271:44-52. DOI
21. Zhang X, Hu H, Tang D, Zhang C, Fu J, Zhao P. Magnetic flexible tactile sensor via direct ink writing. *Sens Actuator A Phys* 2021;327:112753. DOI
22. Ma Z, Wang Q, Wu Z, et al. A superconducting-material-based maglev generator used for outer-space. *Adv Mater* 2022;34:e2203814. DOI
23. Ali B, Ayub MA, Yussof H. Characteristics of a new optical tactile sensor for interactive robot fingers. *Int J of Soc Robotics* 2012;4:85-91. DOI
24. Takahashi H, Nakai A, Thanh-vinh N, Matsumoto K, Shimoyama I. A triaxial tactile sensor without crosstalk using pairs of piezoresistive beams with sidewall doping. *Sens Actuator A Phys* 2013;199:43-8. DOI
25. Engel J, Chen J, Liu C. Development of polyimide flexible tactile sensor skin. *J Micromech Microeng* 2003;13:359. DOI
26. Mo Y, Han H, Liu Y, et al. A tactile sensor based on piezoresistive effect and electromagnetic induction. *Sens Actuator A Phys* 2022;344:113716. DOI
27. Sun X, Sun J, Li T, et al. Flexible tactile electronic skin sensor with 3D force detection based on porous CNTs/PDMS nanocomposites. *Nanomicro Lett* 2019;11:57. DOI PubMed PMC
28. Choi W. Polymer micromachined flexible tactile sensor for three-axial loads detection. *Trans Elect Electron Mater* 2010;11:130-3. DOI
29. Dong Z, He Q, Shen D, et al. Microfabrication of functional polyimide films and microstructures for flexible MEMS applications. *Microsyst Nanoeng* 2023;9:31. DOI PubMed PMC
30. Noda K, Hoshino K, Matsumoto K, Shimoyama I. A shear stress sensor for tactile sensing with the piezoresistive cantilever standing in elastic material. *Sens Actuator A Phys* 2006;127:295-301. DOI
31. Shen D, Jiang Y, Ma Z, et al. Bio-inspired flexible airflow sensor with self-bended 3D hair-like configurations. *J Bionic Eng* 2022;19:73-82. DOI